Specific metrics for direct adiabatic cooling of industrial buildings and climate adaptation

Antoine Breteau, Emmanuel Bozonnet, Patrick Salagnac, Jean-Marie Caous

Energy & Buildings 332 (2025) 115472

Contents lists available at ScienceDirect

Energy & Buildings

journal homepage: www.elsevier.com/locate/enb

Specific metrics for direct adiabatic cooling of industrial buildings and climate adaptation

Antoine Breteau [a,b], Emmanuel Bozonnet [a,*], Patrick Salagnac [a], Jean-Marie Caous [b]

[a] LaSIE (UMR CNRS 7356) - La Rochelle University, Av. Michel Crépeau, 17000 La Rochelle, France
[b] BLUETEK, ZI Nord les Pins, 37230 Luynes, France

ARTICLE INFO

Keywords:
Passive cooling
Evaporative
Adiabatic cooling
Resilience
Comfort
Simulation

ABSTRACT

This paper presents an analysis of the performance of a direct evaporative cooling system incorporated into an industrial building, evaluated in various climates and weather conditions. This system is a simple and economical cooling solution widely used in industrial buildings that combines ventilation and water evaporation cooling. We characterized the system operation through the development of a coupled numerical model of the system and a typical industrial building, in a Mediterranean climate, in the mid-term horizon of 2050. A comparison without any system showed a 74 % reduction in degree-hours of thermal discomfort. Analysis of the building operation shows a predominance of nighttime free cooling, while the adiabatic operates during the occupancy hours. We compared the performance in four different locations, taking into account future weather and heatwaves. The system performed better in hot and dry climates if we consider only the thermal discomfort based on degree-hours, with a 48 % reduction in Abu Dhabi, compared to 41 % in Singapore. However, we observed very different tendencies with water consumption and cooling efficiency: with a cooling efficiency ratio to water use of 22.46 °Ch/m^3 in the equatorial climate, which is almost double that obtained in the dry and arid climate. Arid climates were the most appropriate in terms of energy consumption. In Abu Dhabi, the performance (0.24 °Ch/kWh) was 13 % higher than in an equatorial climate such as Singapore. The results also show that the system performs better under future weather conditions for all the locations studied. Under future conditions, the cooling gain per unit of water consumed rose to 1.48 °Ch/m^3, while the thermal escalation factor decreased by 0.054 points. These results highlight the ability of the system to effectively reduce thermal discomfort, while revealing trade-offs between thermal efficiency, energy consumption and use of water resources. This analysis underlines the relevance of the system to current and future climate challenges.

1. Introduction

On January 12, 2024, the World Meteorological Organization (WMO) officially declared that 2023 was the warmest year on record. The global average annual temperature was 1.5 °C above pre-industrial levels [1]. Human activities are driving the rise in temperature, particularly the extensive use of air conditioning. This solution, increasingly popular for cooling buildings during heatwaves [2], is also a significant contributor to global warming. Air conditioning (with refrigerants) accounts for 7 % of the industrial building sector's greenhouse gas emissions [3]. Adiabatic cooling systems are an alternative to air conditioners that can help mitigate the impacts on global warming and overheating in buildings. This technique was considered for the resilient cooling of buildings in the work of the IEA (International Energy Agency), annex80 [4]. In contrast to air conditioning units (AC), this technology does not use refrigerants, and consumes a significantly lower amount of electrical energy than conventional AC units [5–7]. A typical evaporative cooling system consists of a watered porous material which supplies fresh air after passing through this watered media [8,9]. Water is sprayed onto the upper edges of the pads and then distributed evenly by gravity and capillarity. Falling water is recycled from the water basin by a pump. The system is adiabatic as the air transformation is isenthalpic (no external energy is needed except for the water and fan pumps). The adiabatic evaporation of water due to the influx of hot dry air increases humidity while decreasing air temperature. Direct adiabatic systems deliver this refreshed humid air to the indoor environment, while indirect adiabatic systems prevent humidity buildup by adding an air-heat exchanger [10]. More complex adiabatic cooling systems combine both indirect and direct systems to improve

* Corresponding author.
E-mail address: emmanuel.bozonnet@univ-lr.fr (E. Bozonnet).

https://doi.org/10.1016/j.enbuild.2025.115472
Received 3 December 2024; Received in revised form 3 February 2025; Accepted 12 February 2025
Available online 13 February 2025

Nomenclature

Latin letters [Unit]

AWD	Ambient Warmness Degree [°C]
C	Energy consumption [kWh]
CDD	Cooling Degree Day [°C.h]
DH	Overheating Degree Hours above an operative temperature threshold [°C.h]
IOD	Indoor Overheating Degree [°C]
p	Air pressure [Pa]
PMV	Predicted Mean Vote [-]
Q_v	Volume flow rate [m^3/h]
R_e	Evaporative heat resistance for thermal comfort [m^2.Pa/W]
RH	Relative humidity [%]
*SET**	Standard Effective Temperature [°C]
SETH	Overheating Degree Hours above a *SET** threshold [°C.h]
T	Temperature [°C]
t	Time [h]
U_w	Heat transmission coefficient of windows [W/(m^2.K)]
v	Air velocity [m/s]
V_w	Volume of evaporated water [L]
w	Humidity ratio [kg_w/kg_a]

Greek symbols

ε	Saturation effectiveness [%]
φ	Heat flux [W/m^2]
α	Overheating escalation factor [-]

Subscripts

a	Air
AI	Indoor air
AO	Outdoor air
ASH	Humid supply air
cl	Clothing
mr	Mean radiant
op	Operative
ref	Reference
sk	Skin
sp	Set point
vs	Saturated vapor
w	Water
wb	Wet bulb

dynamically the performance with the system operation [11–13]. There are hybrid systems that combine an adiabatic cooling system with a conventional mechanical cooling system, which improves the efficiency of the conventional system. For example, an adiabatic cooling system can be used as a pre-cooling unit for a steam compression cooling system [14,15]. This combination increases the performance of the steam compression cooling cycle while reducing energy consumption.

Adiabatic cooling systems are particularly effective in hot and dry climates, as shown in the study by Chiesa et al. [16] which showed a 35 % cooling effect quantified with overheating degree-hours (*DH*) in a Mediterranean climate (Eilat in Israel). Many studies have demonstrated the performance of simple direct adiabatic systems in reducing indoor temperature, including that of Morgado et al. who demonstrated that a direct system could maintain a building at a comfortable temperature 48 % of the time in the month of June in Tarragona, Spain [11,17–20], while also increasing indoor humidity [19]. These systems are often considered as a practical alternative in large industrial buildings. This specific use for cooling industrial buildings can be explained by their environmental performance and their low energy consumption [11], and also their simplicity [12]. The main scientific challenge addressed here is the performance of direct adiabatic cooling (DEC) systems in industrial buildings, and more specifically:

- the dynamics of this performance throughout the year;
- the impact of climate change;
- the possible adaptation of these systems for various climates.

The literature review [4–12] highlighted the very small number of papers dealing with these specific direct adiabatic systems in an industrial building context, despite the fact that there are still challenges concerning the complex variations in the energy and thermal comfort performance of these systems in different climate contexts, and their water consumption. Considering their resilience to extreme weather events and the effects of climate change, we propose in this paper to address these research gaps with the use of a more complex and precise definition of thermal comfort performance with the standard effective temperature (*SET**), and its variation with fan energy and water consumption. Previous studies examined only the degree-hours results based on the operative temperature [16], or indoor air temperature and relative humidity [21], or the effective temperature (*ET*), as in Camargo and al. [22]. In addition, we present a numerical model of the system operating in an industrial building. Moreover, our numerical approach allows a wider approach to the operation of these systems in a building compared to more specific studies on the detailed experimental analysis of the system [23,24], or based on a simplified theoretical model [25,26].

The main objective of this paper was to evaluate these systems through specific performance indicators in order to better understand their efficiency in various environments, their influence on occupant comfort and their resource consumption. The article also analyzes their behavior in the context of climate fluctuations and demonstrates their ability to adapt to climate change.

In this work, we analyzed a typical industrial building, and the operation of a direct adiabatic system was first characterized for the Carpentras (France) Mediterranean climate, encompassing climate change up to 2050. In the proposed methodology, we defined six specific KPIs (key performance indicators) to assess the performance of the system for thermal comfort, climate resilience, and water and energy consumption. This analysis focused on the system operation and its complementarity with ventilative cooling. We carried out a parametric study and then investigated the influence of climate on the KPIs in four typical climates (Mediterranean, continental, subtropical, and equatorial), which gives a clear overview of the direct evaporative cooling system applicability in the industrial sector. Finally, we assessed the impact of climate change by comparing the system performance under historical and future climates.

2. Case study

2.1. Typical industrial building

The building studied is representative of a typical industrial building, a warehouse without any specific process that can be adapted to any location and climate zone. It is a steel structure with a floor area of 36 × 36 m^2 and 8 m high. Fig. 1 and Fig. 2 show the building used for this study.

The building stores merchandise (paperboard, metal and pallet boxes) on metal shelves. The vertical walls and the roof are made of two 2 mm thick steel claddings, covering a 5 cm thick layer of rock wool. The lower floor is a 20 cm concrete slab that rests directly on the ground

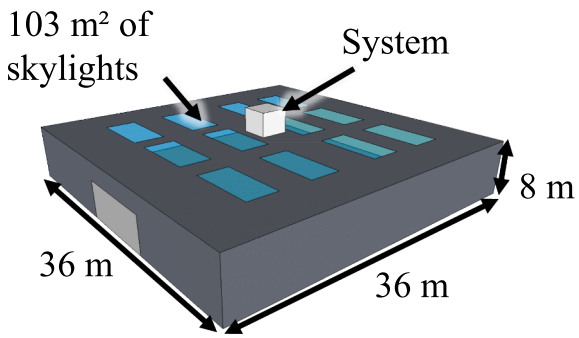

Fig. 1. Diagram of the building.

Fig. 2. Picture of the building.

without insulation. The building is equipped with skylights (U_w = 2.82 W/(m^2.K)) evenly distributed on the roof; this window area represents a surface of 103 m^2 (8 % of the roof surface). The roof has a solar reflectance of 0.3, and a thermal emissivity of 0.9. The infiltration rate was determined from the air permeability, 2.6 (m^3/h)/m^2 under 4 Pa, which is typical for medium watertightness [27]. Required airflow during occupied hours is 45 (m^3/h)/occ [28]. The occupancy density of this type of building is low, 60 m^2/occ in our case study. Thermal discomfort hours were determined during the occupancy period, from 7:00 AM to 10:00 PM, except on Sundays. This schedule was chosen to coincide with the working hours of the people who work at the plant. The building ventilation was designed to maintain the building at a positive pressure during occupied hours, which limits infiltration, especially when the direct evaporative cooling system is operating at a much higher flow rate than required by the sanitary rate.

The internal thermal inertia of the building is mainly due to storage (paperboard, metal and pallet boxes) on metal shelves (Fig. 3).

The thermal inertia of the shelves, merchandise and partitions was considered as an additional internal mass of the building zone. For this case study, 11 storage racks were evenly distributed, 2 m between each rack, with a volume of 6 m in height, 31 m in length and 1 m in width. These racks occupied a floor area of 341 m^2, i.e. 26 % of the total building area.

2.2. Direct evaporative cooling system and free cooling mode

A direct adiabatic cooling system composed mainly of wet pads, a fan and a pump, were installed on the warehouse roof (Fig. 4).

The effectiveness of the system depends on outside conditions (air outdoor AO). The system blows humid air into the building (ASH), which impacts the conditions inside the building (air indoor AI), in particular the comfort of the occupants. This system can operate in two ways. In the **adiabatic** mode, the air is cooled by the evaporation of water, thus lowering the temperature of the air blown into the space. In the **free-cooling** mode, the fan operates without air humidification, when the outside air is sufficiently cool. Unlike the adiabatic mode, this mode has the advantage of preventing humidity buildup inside. The free-cooling and direct adiabatic mode regulation were then adjusted with indoor and outdoor temperature sensors according to Table 1.

The system uses a two-mode control system where the fan adjusts its air flow rate according to a proportional range of 2 °C. In free-cooling mode, this range was determined by two deviations: firstly, the difference between the indoor temperature (T_{AI}) and a specific setpoint ($T_{AI}-T_{sp,fc}$), and secondly, the difference between the outdoor temperature (T_{AO}) and the indoor temperature ($T_{AO}-T_{AI}$). In adiabatic mode, the control was based on a further deviation between the indoor temperature (T_{AI}) and a different setpoint ($T_{AI}-T_{sp,ad}$), as well as on the difference between the outdoor wet bulb temperature (T_{AI}) and the indoor temperature ($T_{AI}-T_{wb,\ AO}$). This approach optimizes system efficiency by making the most of temperature differences between the inside and outside to maximize available cooling potential [29,30].

2.3. Climate zones and adiabatic system sizing

In order to study the climate resilience of the system, and to highlight its performance variations, we chose four very different climates from the generated extreme weather files in the IEA annex 80 methodology [31,32]. The climates studied have four distinct characteristics. The Mediterranean climate, represented by Carpentras (France), is marked by hot, dry summers and mild winters. The continental climate, observed in Paris (France), is characterized by fairly hot summers and moderate winters. The arid subtropical climate, such as in Abu Dhabi (United Arab Emirates), is hot and dry throughout the year. Finally, the equatorial climate (Singapore) is defined by stable temperatures ranging from 22 to 32 °C, a high relative humidity of 70 to 80 % and cool nights. The typical historical weather data are based on 20 years of meteorological data (Table 2).

In this article, we used historical (2001 to 2020) and midterm periods (2041 to 2060), taking a typical year with extreme heatwaves for each period, as defined by the annex 80 method [33]. The midterm climate given by this method was provided by Cordex data [32] and uses

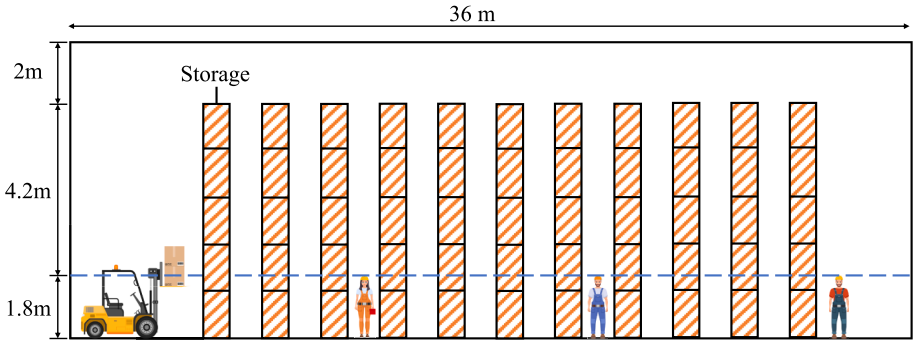

Fig. 3. Storage rack distribution in warehouse case study for internal thermal inertia.

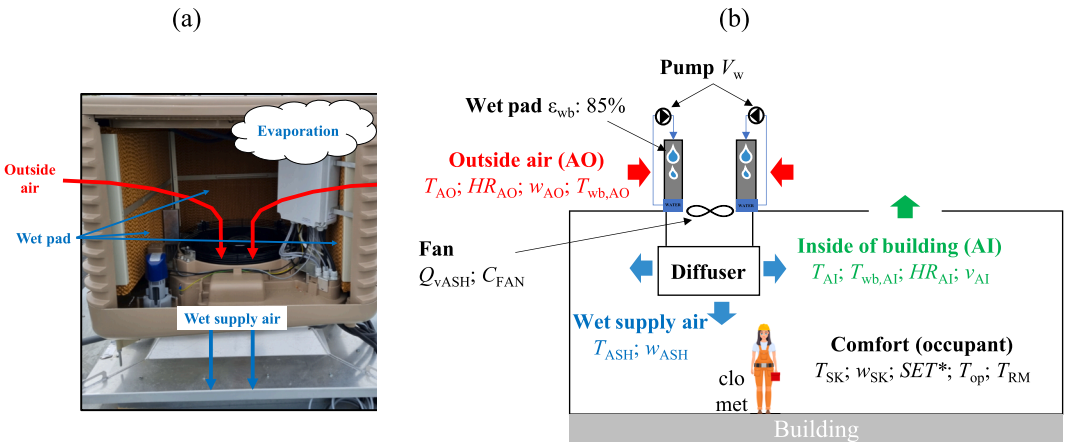

Fig. 4. Direct adiabatic system (a), and system integration onto the building (b).

Table 1
Indoor and outdoor temperature conditions.

	Free cooling conditions		Adiabatic conditions	
Air temperature conditions	Indoor	Outdoor	Indoor	Outdoor
Occupancy hours	$T_{AI} > 22$ °C ($T_{sp,fc}$)	$T_{AO} < T_{AI}$	$T_{AI} > 24$ °C ($T_{sp,ad}$)	$T_{wb,\ AO} < T_{AI}$
Unoccupied hours	$T_{AI} > 19$ °C ($T_{sp,fc}$)	$T_{AO} < T_{AI}$	$T_{AI} > 28$ °C ($T_{sp,ad}$)	$T_{wb,\ AO} < T_{AI}$

Table 2
Climate characterization.

Locations	Carpentras (France)	Paris (France)	Abu Dhabi	Singapore
Climates	Mediterranean (3A)	Continental (4A)	Arid subtropical (0B)	Equatorial (0A)
CDDs [°C.h] ($T_b = 26$ °C)	7723	1691	47,298	33,678
Cooling season ($T_b = 26$ °C)	May 1 to October 15	May 1 to October 15	April 1 to November 15	February 28 to November 1
Average daily maximum outdoor temperature [%]	34.2	34.6	43.5	34
Average daily outdoor relative humidity [%]	64	70	59	84

the high emission scenario for future climate change.

The correct sizing of the direct adiabatic system is crucial for our study in terms of energy performance in the dynamic mode, and strongly depends on the building location. So, the number of adiabatic boxes installed on the roof of the warehouse was correlated with the maximum airflow required in nominal conditions, which we determined for our case study under the various climate zones (Table 3).

Table 3
System airflow sizing (Q_{vASH}^{MAX}) for the industrial warehouse, and various climate zones.

Locations	Carpentras (France)	Paris (France)	Singapore	Abu Dhabi
Design airflow Q_{vASH}^{MAX} [m^3/h]	22 000 (2.1 ACH)	22 500 (2.1 ACH)	23 000 (2.2 ACH)	21 500 (2.1 ACH)

We determined the optimum steady-state airflow rate Q_{vASH}^{MAX}, taking into account the typical extreme outdoor temperatures for each climate zone, and the equivalent indoor temperature *SET** was computed for various airflows in order to size the fan and the number of adiabatic boxes. Fig. 5 illustrates this problem with the typical case of Carpentras (Mediterranean climate). The problem here is that even with an infinite flowrate ($Q_{vASH=\infty}$), the minimum achievable cooling, given by $SET^*(Q_{vASH=\infty}) = SET^*_{min}$, is generally above the target setpoint in extreme conditions (26 °C). Moreover, even if this target could be reached, the design airflow might be prohibitive in terms of fan energy consumption, and a reasonable compromise has to be reached in the system sizing method.

So, we defined the design airflow Q_{vASH}^{MAX} with a reasonable value, which is the airflow that provides a cooling effect of (2 / 3) × [$SET^*(Q_{vASH} = 0) - SET^*(Q_{vASH=\infty})$] in steady-state conditions. The choice of the 2/3 coefficient was based on an analysis of the curve obtained. Actually, beyond this limit, the increase in airflow no longer produces a significant cooling gain with regard to the potential *SET** decrease. The key element in this choice is the relationship between the gain in *SET** and the increase in airflow. The sizing approach of the system adopted here in order to be able to compare it under all climates, is to determine in the same systematic way the optimum maximum fan power required to achieve a balance between the indoor comfort gain provided by the system and its energy consumption.

3. Model and methodology

3.1. Adiabatic system and building model

The thermal simulation was developed using the TRNSYS software, which has the advantage of being very modular when incorporating the equations of our direct adiabatic system into the regulations and the detailed building model in the software.

The evaporative cooling process reduces the air temperature and consumes water. The sensible heat of hot air is converted to latent heat as the air passes through a wet media, which draws heat from hot air to evaporate water that is converted to vapor in the air supplied to the building. This process reduces the air temperature (T_{AO}, dry bulb temperature) while increasing its humidity, keeping enthalpy constant in an ideal adiabatic cooling scenario. The lowest achievable temperature corresponds to the thermodynamic wet bulb temperature ($T_{wb,AO}$) of the incoming air. Saturation efficiency is measured from the ratio between the actual decrease in T_{AO} and the maximum theoretical decrease in $T_{wb,\ AO}$ that could be achieved if cooling were fully efficient, with saturated outlet air.

The direct adiabatic model supposes a constant saturation efficiency

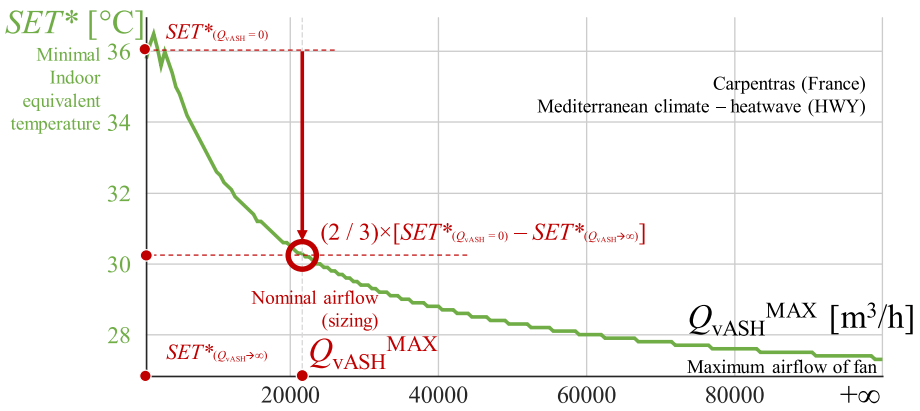

Fig. 5. Sizing methodology for the fan nominal airflow illustrated for the typical heatwave year of Carpentras (Mediterranean climate).

$\varepsilon_{wb} = 0.85$ [29], and is defined in relation to the outdoor air temperature T_{AO}, supplied airflow T_{ASH}, and wet bulb temperature $T_{wb,\ AO}$; see equation (1).

$$\epsilon_{wb} = 100\frac{T_{AO} - T_{ASH}}{T_{AO} - T_{wb,\ AO}} \quad (1)$$

The constant efficiency simplification could be refined depending on the variation in air velocity and exchange area between the airflow and the watered media [30]. The air temperatures can be represented on a psychrometric chart (Fig. 6).

This graph shows that the air transformation was isenthalpic. The saturation efficiency ε_{wb} was calculated using the cooling potential between the dry bulb outdoor air temperature and the wet bulb outdoor air temperature.

This adiabatic system was then coupled to the building model in TRNSYS, as represented on Fig. 7.

The building model is based on a single air node per zone, taking into account the various heat transfers (radiative, conductive and convective) between the building walls, interior and exterior.

In this study, the ground thermal model takes into account both the thermal mass of the soil, and the heat losses with the outdoor environment through the definition of the slab on ground equivalent thermal bridge [34,35].

The thermal mass of the interior equipment such as cardboard boxes, metal shelves or other materials present in the building is taken into account through their thermal properties (density, thermal conductivity, thermal mass capacity). Finally, internal heat gains, including those from occupants and electrical equipment, are modelled as heat flows [W/m^2], taking into account convective and radiative contributions. The coupling procedure is iterative at each time step in order to have a strong coupled simulation in line with the regulation of the system, which depends on the building response itself and the 15 min time step. Thanks to this numerical model, we were able to evaluate the performance of this system through different indicators of comfort, performance and resilience.

3.2. Key performance indicators (KPI)

In this paper, the objectives were achieved using a variety of comfort and resilience indicators. According to ASHRAE 55-2013 [36], thermal comfort is defined as "that state of mind which expresses satisfaction with the thermal environment" and is generally assessed subjectively. Thermal comfort is described using three main approaches: physiological, physical and psychological [37]. The thermal environment and the perception of thermal comfort under steady-state conditions depend on environmental factors such as indoor air temperature, mean radiant temperature, air velocity and relative humidity, alongside behavioral aspects such as clothing insulation and metabolic heat rate. In our approach, we used the operative temperature T_{op}, which is widely used in most building regulations, and the Standard Effective Temperature *SET**, which is a much more precise definition of thermal discomfort, especially for direct adiabatic cooling and variations in humidity. A summary of the indicators used is presented in Table 4.

The T_{op} indicator was developed in the 1930s [38] and takes into account the convective and radiative effects of the interior. The operative temperature is defined as the uniform temperature of an imaginary black enclosure in which an occupant would exchange the same amount

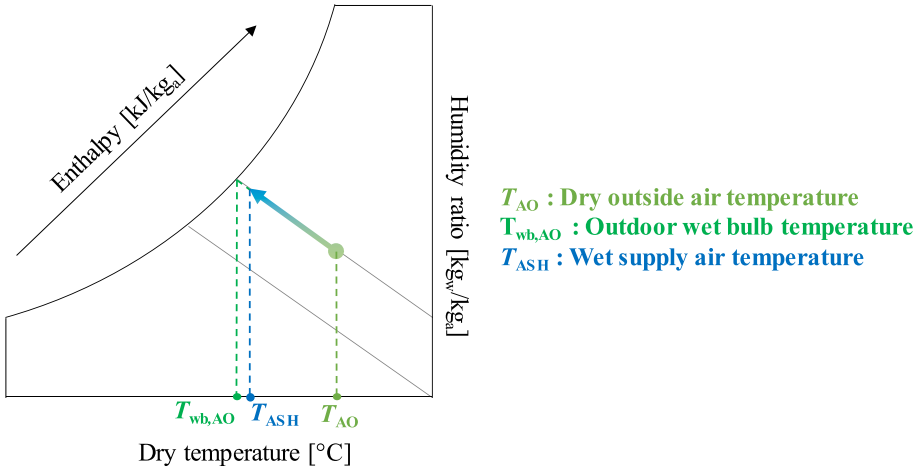

Fig. 6. Psychrometric chart.

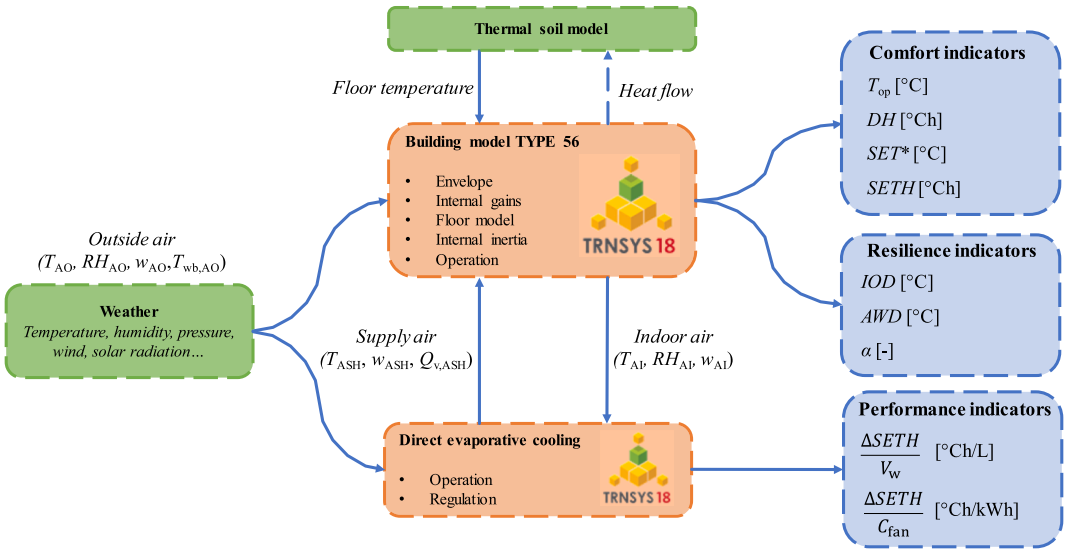

Fig. 7. TRNSYS model.

Table 4
KPIs.

Analysis context	KPIs	Physical value	unit	Normalized(*) KPI value [%]
Comfort	Overheating Degree Hours above a *SET** threshold	*SETH*	°C.h	$1-\frac{SETH_{sys}}{SETH_{ref}}$
	Overheating Degree Hours above an T_{op} threshold	*DH*	°C.h	$1-\frac{DH_{sys}}{DH_{ref}}$
	Daily Maximum Perceived Cooling	$SET^*_{dailymax}$	°C	$1-\frac{SET^*_{dailymax,sys}-28}{SET^*_{dailymax,ref}-28}$
Resilience	Overheating escalation factor	α	–	$1-\frac{\alpha_{sys}}{\alpha_{ref}}$
Performance	Reduction of overheating by the system compared to fan consumption	$\Delta SETH/C_{fan}$	°C.h/kWh	$1-\left(\frac{1}{\frac{\Delta SETH}{C_{fan}}_{max}}\times\frac{\Delta SETH}{C_{fan}}\right)$
	Reduction of overheating by the system compared to the volume of water evaporated	$\Delta SETH/V_w$	°C.h/m^3	$1-\left(\frac{1}{\frac{\Delta SETH}{V_w}_{max}}\times\frac{\Delta SETH}{V_w}\right)$

(*) 100% indicates the best system performance.

of heat by radiation and convection as in the non-uniform real environment [39]. This temperature can be determined by satisfying two conditions ($v_{AI} < 0.2$ m/s and $|T_{mr}-T_{AI}| < 4$ °C) (2).

$$T_{op} = \frac{T_{AI} + T_{mr}}{2} \tag{2}$$

From ASHRAE-55, the *SET** temperature is defined as an operating temperature of a reference environment that would cause the same physiological responses as the real environment. The *SET** is defined as the equivalent of the dry-bulb temperature of an isothermal environment at 50 % relative humidity where the occupants would have standardized clothing for the activity in question, which would have the same thermal stress (skin temperature) and thermoregulatory constraint (skin wetness) as in a reference environment. Skin temperature T_{sk} and skin wetness w_{sk} are derived from a two-node model of human physiology (Pierce's model) [40], which gives the total heat flux density φ_{sk} for the convective, evaporative and radiative contributions of the skin (3).

$$\varphi_{sk} = \frac{1}{R_a + R_{cl}}(T_{sk} - SET^*) + \frac{w}{R_{ea} + R_{ecl}}(p_{sk} - 0.5p_{vs}(SET^*)) \tag{3}$$

R_{cl} and R_a correspond to the heat resistance of the clothing and air. R_{ecl} and R_{ea} correspond to the evaporative heat resistance of the clothing and air. The saturation vapor pressure difference is given by p_{sk} at skin temperature, and $p_{vs}(SET^*)$ at *SET** as the air temperature.

The cumulative thermal discomfort can be characterized by the cumulative degree-hour above a threshold $T_{i,lim}$, which gives a standardized assessment of overheating with T_{op}. For each equivalent temperature T_i, T_{op} or *SET**, the discomfort limit can be defined from building regulations or equivalent neutral discomfort limits in order to compute the discomfort degree-hours *DH* or *SETH* as defined by equation (4).

$$DH \text{ or } SETH = \sum_{h=1}^{n}\left(T_i - T_{i,lim}\right)_{T_i > T_{i,lim}} \tag{4}$$

The temperature threshold $T_{i,lim}$ for T_{op} and *SET** were determined by an equivalence method using the PMV indicator [41]. We chose a PMV indicator between −0.5 and 0.5 for a neutral thermal sensation. This choice was supplemented by several hypotheses ($v_{AI} = 0.2$ m/s, metabolism 1.4 met, clothing insulation 0.59 clo). According to the psychometric comfort diagram defined by ASHRAE, an operating temperature T_{op} (26 °C) and its equivalent in *SET** (28 °C) was determined [36].

For the study of resilience, S. Attia et al. [42] showed that the impact of climate change on the risk of overheating in buildings with different cooling strategies can be assessed using the methodology proposed by M. Hamdy et al. [43]. The method is based on three indicators: *AWD*,

IOD and α.

The *IOD* is an average overheating temperature which is the sum of the positive values of the difference between the operating temperature (T_{op}) of the zone and the limit comfort temperature of the same zone (26 °C), averaged over the sum of the total number of occupied hours (N_{occ}).

$$IOD = \frac{\sum_{i=1}^{N_{occ}} \left(T_{op,i} - 26\right)\Delta t}{\sum_{i=1}^{N_{occ}} \Delta t_i} \quad (5)$$

where Δt is the time step [h], i is the occupation hour counter taking into account the calculation period.

AWD is used to quantify the severity of outdoor thermal conditions. It's the positive sum of the difference between the outdoor air temperature T_{AO} and the base temperature T_b reduced to the number of hours of occupation. The choice of the base temperature is context specific, depending on the building typology and the climate.

$$AWD = \frac{\sum_{i=1}^{N_{occ}} (T_{AO} - T_b)\Delta t_i}{\sum_{i=1}^{N_{occ}} \Delta t_i} \quad (6)$$

where the base temperature T_b is set at 26 °C. A value of $T_b = T_{lim}$ was chosen because the α indicator is designed to take the value 1 to distinguish between resilient ($\alpha < 1$) and non-resilient ($\alpha > 1$) buildings. With this choice, we obtained a linear regression of the α indicator, which simplified the interpretation of the resilience of the building [44].

The α indicator was used to evaluate the resistance of a building to climate change and the associated risk of overheating. It corresponds to the slope of the regression curve between *IOD* and *AWD*.

$$\alpha = \frac{IOD}{AWD} \quad (7)$$

The α indicator shows the potential of cooling technologies to withstand the effects of climate change. $\alpha < 1$ means that the building will be able to cope with the external thermal stress in the long term and $\alpha > 1$ means that the building will be unable to cope with the external thermal stress in the long term.

The $\Delta SETH/C_{fan}$ indicator allows an assessment of the ratio of the cooling gains assessed by the *SETH* reduction, and the energy consumption of fan (8).

$$\frac{\Delta SETH}{C_{fan}} = \frac{SETH_{ref} - SETH_{sys}}{C_{fan}} \quad (8)$$

Following the same principle, the $\Delta SETH/V_w$ indicator allows an assessment of the cooling gains in relation to the volume of water evaporated by the system (9).

$$\frac{\Delta SETH}{V_w} = \frac{SETH_{ref} - SETH_{sys}}{V_w} \quad (9)$$

The daily maximum perceived cooling $SET^*_{dailymax}$ indicator is the maximum daily average SET^* temperature over the year. This indicator was evaluated in relation to the comfort limit of 28 °C (optimum value) and the value of the reference case (without the system).

To display these indicators on a radar chart and compare the performance of all indicators, each value was normalized on a scale from 0 % for the base case scenario without the adiabatic system, to 100 % for the best performance. The normalized formulas are shown in Table 4.

4. Results and discussion

The results of the study are presented in three sub-sections, corresponding to the main objectives of the paper: system characterization, climate and location, and climate change. Table 5 provides an overview of the case studies.

Table 5
Summary of case studies.

Main focus	Locations	Weather files	KPIs
System operation	Carpentras (France) – Mediterranean climate	Heatwave year (HWY) at mid-term horizon of 2050	*SETH* *DH* $\Delta SETH/C_{fan}$ $SET^*_{dailymax}$ α
Impact of climate	Continental (Paris – 4A) Mediterranean (Carpentras – 3A) Arid subtropical (Abu Dhabi – 0B) Equatorial (Singapore – 0A)	Heatwave year (HWY) at mid-term horizon of 2050	*SETH* *DH* $\Delta SETH/C_{fan}$ $SET^*_{dailymax}$ α + $\Delta SETH/V_w$
Climate change	Carpentras	Actual and future typical meteorological year (TMY)	

This table provides a summary of the case studies discussed in this paper, highlighting the different parts covered and the data used, such as climate, weather files, and key performance indicators (KPIs).

4.1. Analysis of the system and building operation

For this section, the system was analyzed using the Mediterranean climate of Carpentras (France) with typical scorching weather. The Mediterranean climate was chosen to characterize the system as the warm, arid outdoor conditions are particularly well-suited to the default design of this system. These conditions make it possible to analyze the system operation in a typical environment where it is widely used. The operation of the system was studied, as well as its impact on indoor discomfort.

4.1.1. Weather conditions

Daily and annual variations of ambient air temperature, humidity and solar radiation are given for a heatwave year (HMY) in Fig. 8, using the historical weather data.

The diagram shows that the hot period is in summer (June – September). During this period, the outdoor temperature is the highest, with an average of 29 °C. At the same time, relative humidity decreases to an average of 47 %. The days with the highest average solar radiation are in the summer period (June 1 to September 1), with an average of 103 Wh. The sunniest day during this summer period is the 6th of August, with an average daily solar radiation of 278 Wh.

4.1.2. System operation

First, we characterized the operation of the system over two days at mid-season with hot weather. The building is equipped with a direct evaporative cooling system with a maximum airflow of 22 000 m^3/h (2.1 ACH). Fig. 9 shows the temperature, relative humidity (indoor and outdoor) and the operating mode of the system (adiabatic or free-cooling).

Fig. 9 shows how the system worked based on the indoor and outdoor conditions of the building and also the regulation with the different set temperatures ($T_{sp,ad}$ and $T_{sp,fc}$). By comparing the change in absolute humidity with and without a system, we observed a sudden increase in absolute humidity when starting the adiabatic mode due to air humidification; at the same time the indoor air temperature stabilized. The system was controlled to operate mainly in free cooling mode when the building was unoccupied ($T_{sp,fc}$ lower than $T_{sp,ad}$). This reduced the water consumption of system. The adiabatic mode operated mainly during busy periods because the cooling potential is highest (dry outdoor conditions). With the same approach, we analyzed the system operation for the summer and winter periods. Our results (see Appendix) show intensive (air flow max) use of the system in adiabatic and free-cooling mode during the summer period, while it was not used at all

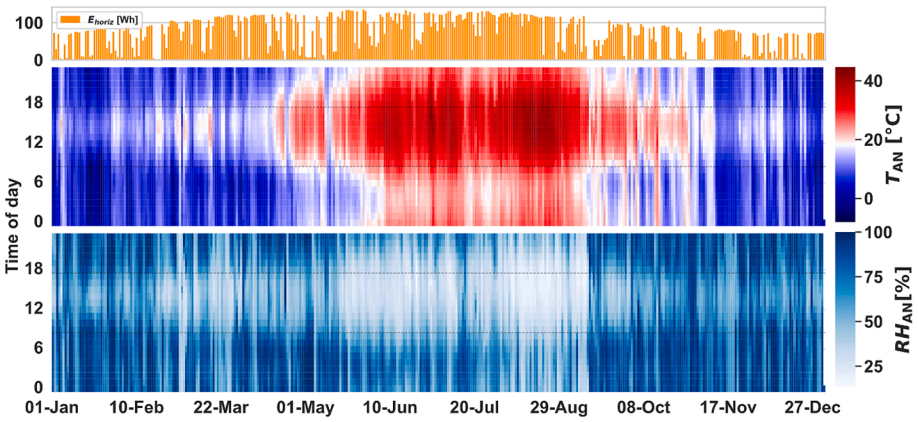

Fig. 8. Outdoor conditions of a Carpentras heatwave (2050).

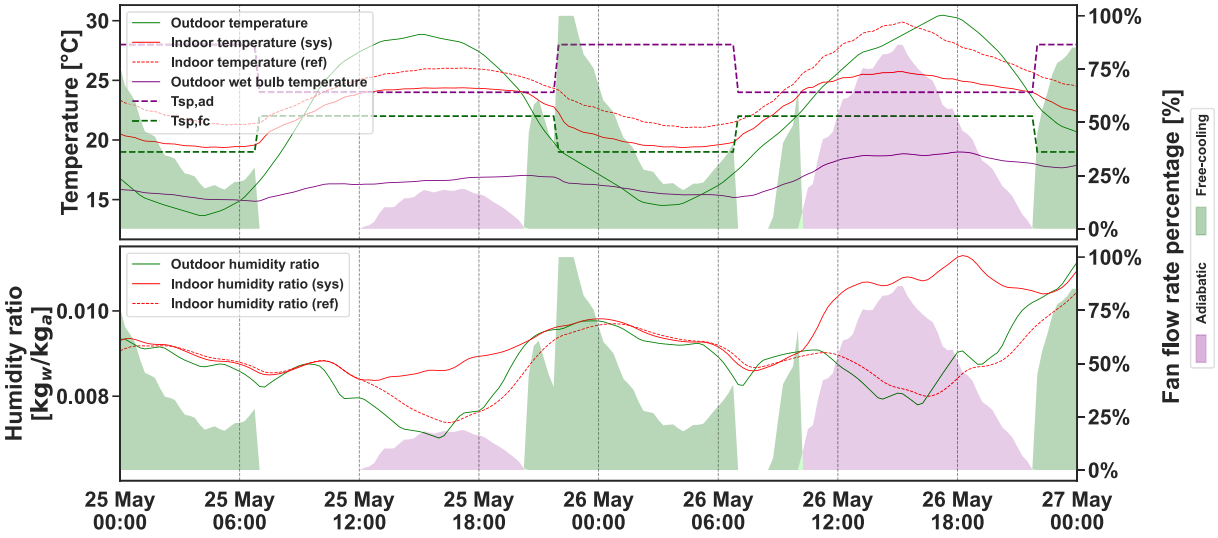

Fig. 9. System operation over 2 consecutive days (mid-season).

during the winter.

Secondly, the operation of both modes of the system was studied. Fig. 10 shows a stacked bar chart representing the average daily power consumption of the system fan and pump (*Cons*) and the average daily evaporated water flow ($Q_{v,w}$). The percentage fan power in each mode is represented by the intensity of the colors as a function of time of the day (ordinate) and day of the year (abscissa).

During this period, the system was in adiabatic mode for 1895 h (55 % of the operating time), compared to 1500 h in free-cooling mode (45 % of the operating time). It can be seen that the free-cooling mode was

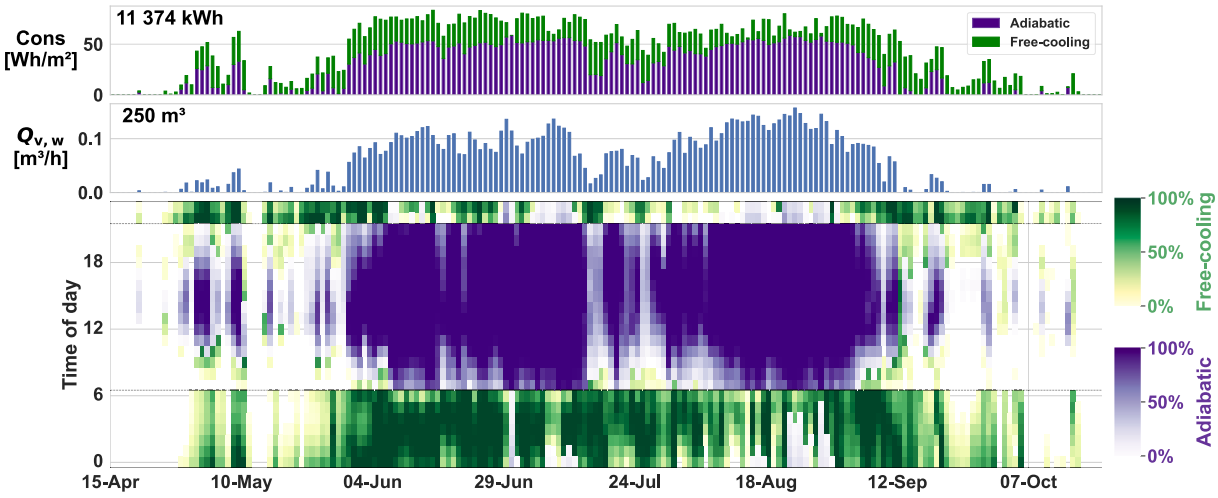

Fig. 10. Operation of the system from April 15 to October 20.

used frequently during periods of inactivity, typically from 10:00 PM to 7:00 AM, with a significant air supply rate, especially during the summer season. It's worth noting that the adiabatic mode was activated during the day, while the free-cooling mode was preferred at night. This observation is the result of an operating strategy dictated by the difference in setpoints during periods of inactivity, set at 19 °C for free-cooling and 28 °C for adiabatic cooling. The adiabatic mode started early in the morning, when the efficiency of free-cooling decreased due to high indoor temperatures. At the same time, variations in the fan and pump consumption were noted based on the duration of use of the different modes. Over the studied period, the total electricity consumption of the system amounted to 11 374 kWh, mainly due to the adiabatic mode (6 708 kWh), free-cooling (4 151 kWh) and hygienic flow (515 kWh).

In this particular climate, the system preferred to use free-cooling to reduce water consumption, given that the daily evaporation rate often exceeded 100 L/h in summer. The total volume of water evaporated was 250 m^3. Including drainage, this volume rose to 474 m^3. The water management in this system relies on various cycles and drainage to efficiently move storage water.

4.1.3. Thermal comfort

The overheating of the *SET** compared to a setpoint temperature limit (SET^*_{lim} = 28 °C) is shown in Fig. 11 based on days and hours of operation with and without the system. Additionally, the difference in this overheating, both with and without the system, is depicted daily in the form of a bar histogram. The results are displayed for the period from 15 April to 20 October, with this selection made for the external conditions conducive to the system's operation.

We observed significant overheating during the hot period (June-September), with a low point at the end of July due to reduced external contributions. There was a substantial reduction with and without the system. In terms of severity, the number of degree-hours without the system per year was 4869 °Ch, whereas with the system, it was 2119 °Ch, representing a 56 % reduction. This reduction is significant at high temperatures (June−July and August), occasionally reaching around 50 °Ch/day. During this period, the average reduction was 14 °Ch/day. These results are different from those of the *DH* indicator, which were calculated using the operative temperature T_{op}, taking into account only the sensitive part (Fig. 12).

If we look at the internal overheating assessed at the operative temperature (T_{op}) (Fig. 12), we notice that it was higher than with the *SET** for an equivalent comfort limit temperature. The severity of this overheating without the system was 9526 °Ch, which is 96 % more than with the *SET**. In this assessment, the system reduced internal overheating by 74 % (2444 °Ch). This reduction is 18 points higher than that achieved with the *SET**. Some days, this reduction could reach 100 °Ch/day. During this time of the year, the average reduction was 39 °Ch/day. These results show that the system helps reduce indoor discomfort, but to a lesser extent when relative humidity is taken into account.

To conclude, we carried out an analysis of indoor discomfort for different configurations. Three scenarios were considered: no system (Reference, red), free-cooling mode (FC, green), and combined adiabatic and free-cooling mode (AD + FC, purple). The absolute values obtained are presented in Table 6:

Table 6 shows that the system performed better when it operated in adiabatic and free-cooling mode (AD + FC) than with free-cooling alone (FC). Using both modes (FC + AD) saved 65 % (*DH*) and 41 % (*SETH*) compared with a system operating with free-cooling only (FC). The $SET^*_{dailymax}$ decreased by 1.5 °C with both modes and by 0.9 °C with only the free-cooling mode. When operating in free-cooling mode only, the system saved 0.15°Ch/kWh, i.e. 0.9°Ch/kWh more than when operating in adiabatic and free-cooling mode. The resilience of the building was very low when the system was not in place ($\alpha \approx 1$). The building was more resilient when the system operated in both modes ($\alpha = 0.24$).

Finally, we plotted the relative values (reference 0 % without the system) of these indicators on a radar chart (Fig. 13).

Fig. 13 shows the system performance as a function of the mode used. We can see that the trend is the same for the relative and absolute values. The graph shows that the surface area where adiabatic and free-cooling were employed (AD + FC) is twice as large as the surface area where only free-cooling was employed (FC). This shows that the system performed better with both modes in operation. The system with the two modes makes it possible to reduce the discomfort (T_{op}) by 74 % in the reference case while with only free-cooling the discomfort was reduced by 25 %. The trend was similar for the *SET**, with a reduction of 56 % of the system with both modes and 26 % with free-cooling only. The system reduced the daily maximum perceived cooling by 26 % with the two modes used and 14 % with free-cooling alone. The reduction in degree hours as a function of fan consumption was greatest when the system was operating in adiabatic and free-cooling mode. It was 36 points lower when only free-cooling was used.

4.2. Impact of climate

This section examines the effect of the climate in which the system is installed. The system operated in both modes (AD + FC). Four locations were chosen because of their different climates: Carpentras, Paris, Abu Dhabi and Singapore. For this study, the weather data used are characteristic of a typical heat wave climate.

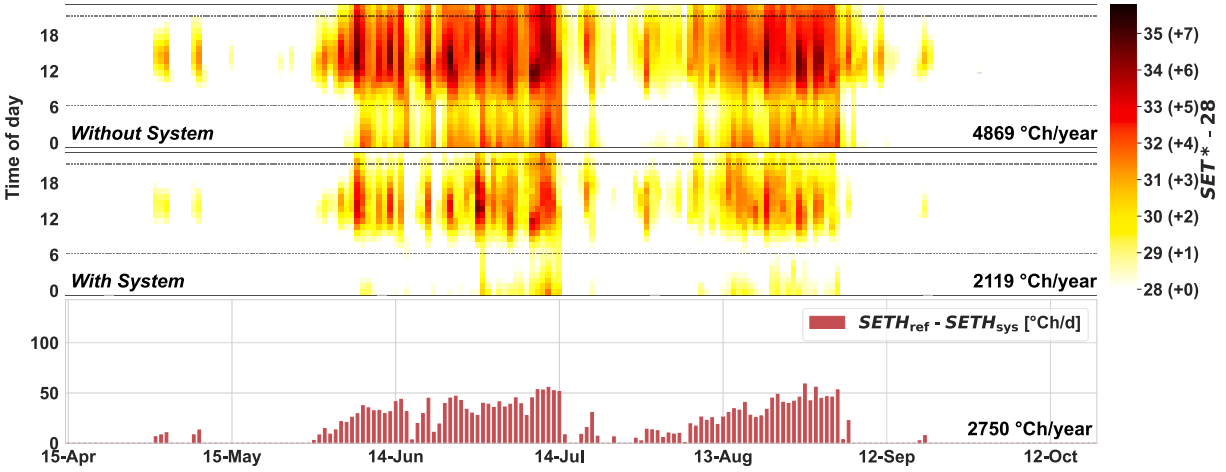

Fig. 11. Interior overheating (SET*−SET^*_{lim}).

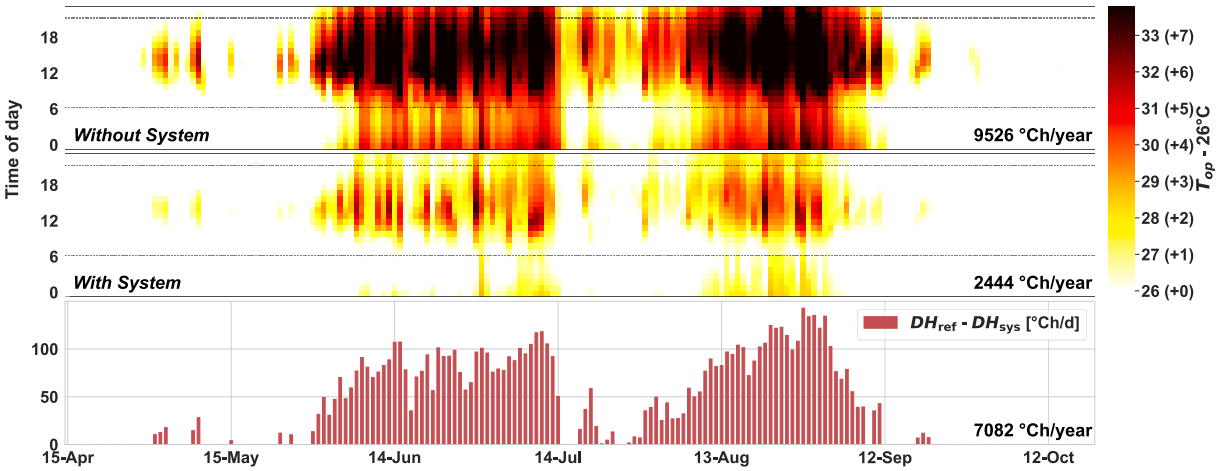

Fig. 12. Interior overheating ($T_{op}-T_{op,lim}$).

Table 6
Absolute values representing the performance of the system for the Carpentras climate.

	Reference	FC	AD + FC
DH [°Ch]	9526	7126	2445
SETH [°Ch]	4870	3596	2119
$SET^*_{dailymax}$ [°C]	33.8	32.9	32.3
$\Delta SETH/C_{fan}$ [°Ch/kWh]	0	0.15	0.24
α [-]	0.94	0.7	0.24

4.2.1. Weather conditions

First, we characterized the external conditions of each location. Different heat maps show the change in outdoor temperature as a function of the day (x-axis) and the time (y-axis).

Fig. 14 shows the significant differences in outdoor temperatures during the year for different locations. We can see many differences for outdoor conditions between continental, Mediterranean and oceanic climates. For Carpentras, the outdoor temperature remained high for a longer period in summer compared to other French locations, with an average outdoor temperature of 17.3 °C throughout the year compared to 14.4 °C in Paris. Carpentras has a drier climate with an average relative humidity of 64 % over the year compared to 70 % in Paris. The hottest climates are Abu Dhabi and Singapore, with an annual average of 30.1 °C and 29.8 °C, respectively. Abu Dhabi's climate is drier than Singapore's, with 59.6 % and 84.5 % average relative humidity, respectively, over the year. The maximum outdoor temperature reached in each city was: 35.8 °C (Singapore), 51.5 °C (Abu Dhabi), 44.6 °C (Carpentras) and 43 °C (Paris). We chose these different climates because they are very different from each other. The effectiveness of the system in reducing summer discomfort will depend on these external conditions.

4.2.2. System operation

Fig. 15 presents the operating time and annual consumption of the fan for adiabatic (purple) and free-cooling (green) modes.

As expected, the operating time and annual consumption of the fan behaved similarly. As illustrated in Fig. 15, the adiabatic mode was employed most frequently in the various climates, with the exception of Paris, where the external conditions are conducive to the free cooling mode. Quantitatively, for the Abu Dhabi climate, the adiabatic mode was used three times more often (6 447 h) than the free-cooling mode (1 862 h), as reflected in the annual fan consumption. This phenomenon is due to the dry climate both at night and during the day in Abu Dhabi. In Carpentras, the consumption scale was much smaller: the fan consumed only 6 632 kWh in adiabatic mode, 1.6 times more than in the free-cooling mode (4 151 kWh). The consumption was lower than for the climate of Abu Dhabi because the climate of Carpentras is similar to that

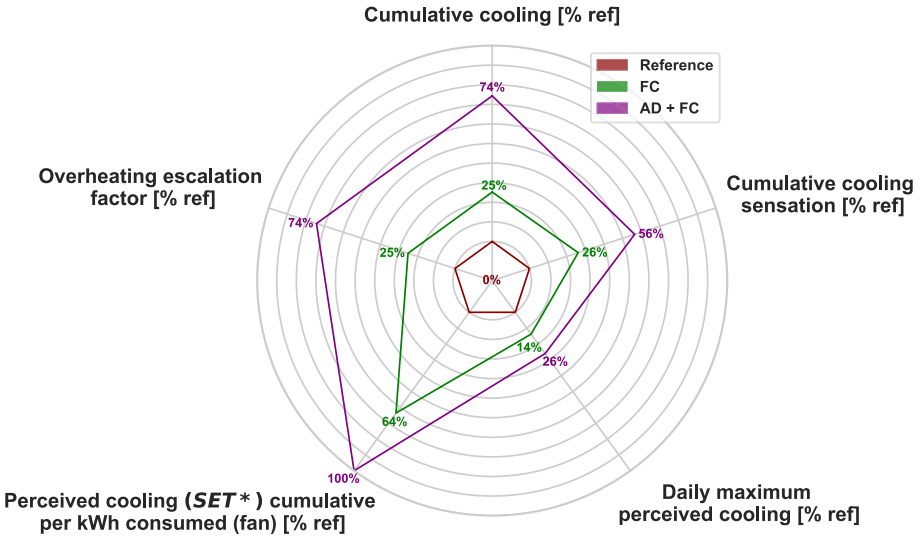

Fig. 13. Radar graph representing the performance of the system for the Carpentras climate.

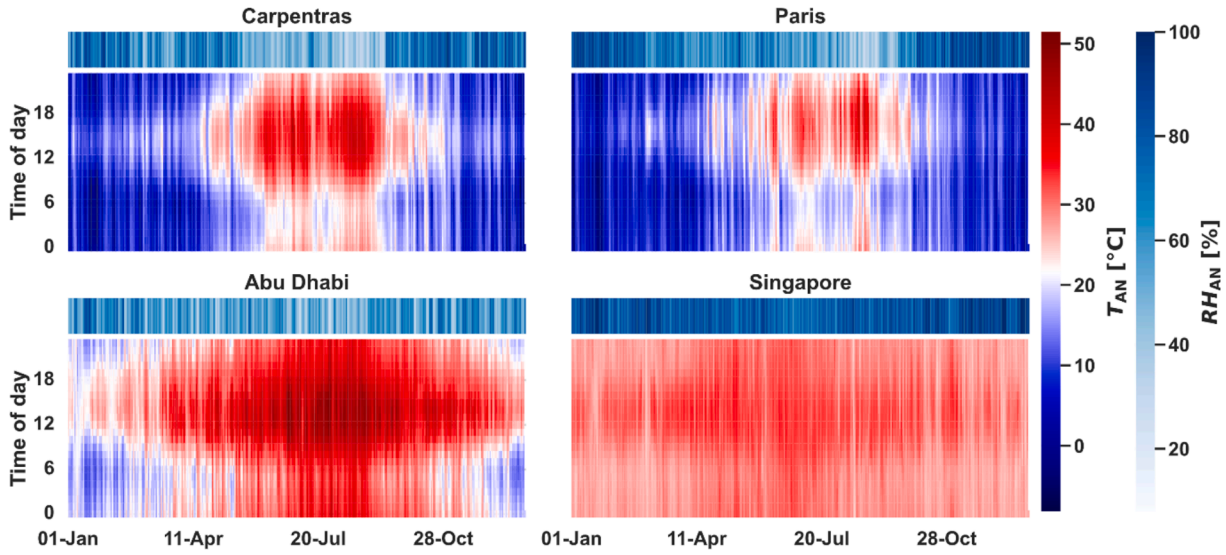

Fig. 14. Change in the annual outdoor temperature for a typical scorching weather year and for different locations.

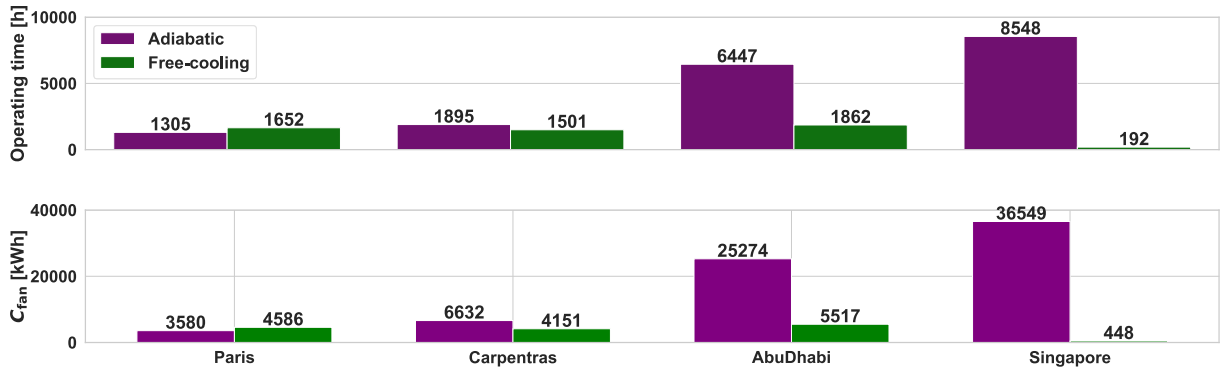

Fig. 15. Operating time and annual consumption of the fan in two modes (AD and FC).

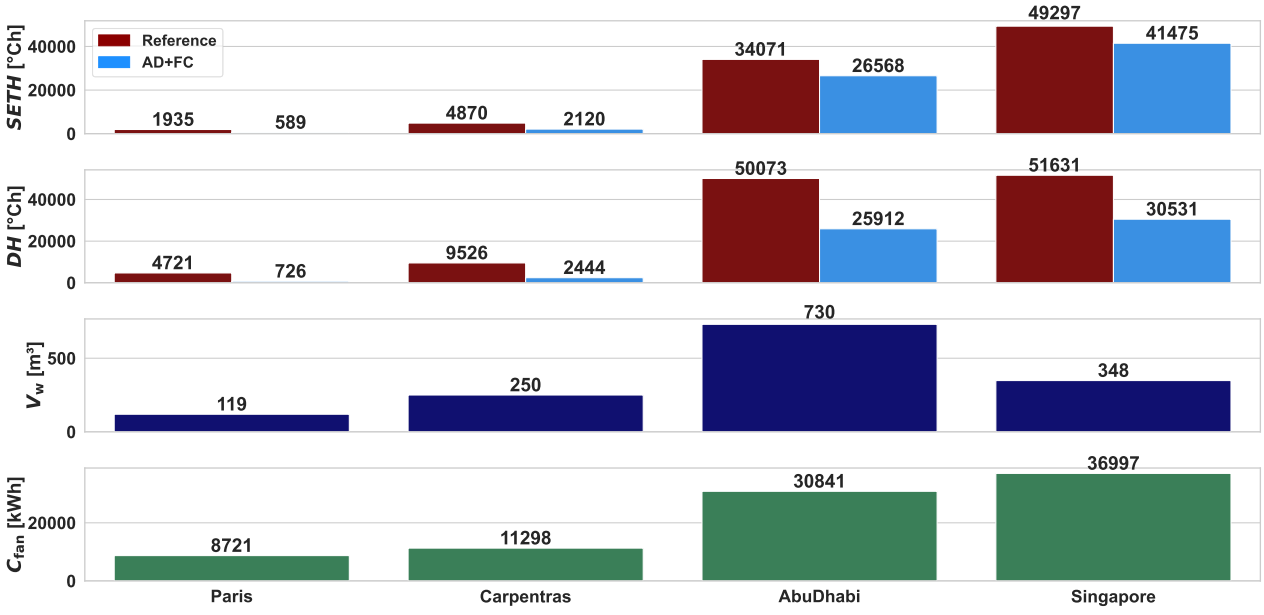

Fig. 16. Quantitative analysis of different indicators (Thermal and performance).

of Abu Dhabi but much less extreme in temperature and a little more humid. For Singapore, which is more humid and hotter, the adiabatic mode was almost always used (98 % of the system's operating time), with an annual consumption of 36 549 kWh compared to 448 kWh for the free-cooling mode.

4.2.3. Thermal comfort

Thermal comfort was assessed using the *SET** temperature and the operating temperature (T_{op}) via the *SETH* and *DH* discomfort degree hours, respectively. The performance of the system was assessed by the volume of evaporated water (V_w) and the power consumption of the fan (C_{fan}) (Fig. 16).

This graph shows a similar trend for each climate for the comfort indicators (*DH* and *SETH*). Paris is the city with the lowest level of discomfort, while Singapore is the city with the highest level of discomfort. Quantitatively, it was observed that the severity of discomfort is more significant in extreme climates (Abu Dhabi and Singapore) compared to the French climate (Paris and Carpentras). It is also noticeable that the impact of the system on this discomfort varied between climates. In terms of *DH* severity, the system reduced discomfort by 84 % in Paris and by 74 % in Carpentras. There was also a difference in severity in terms of *DH* and *SETH*; in general, the severity was higher for *DH*, mainly due to the inclusion of relative humidity in the *SET** calculation. This results in a less significant reduction in discomfort by the system when the severity was calculated using *SET**. Taking the city of Singapore as an example, the reduction in discomfort was 15 % with *SETH* compared to 40 % with *DH*. In terms of severity with *SETH*, the system could reduce overheating by a maximum of 69 % in Paris, while this reduction was 56 % for Carpentras.

We note that in arid climates the system evaporated a lot of water (for example, 730 m^3 was evaporated in Abu Dhabi); this phenomenon of water evaporation through the media is important. In contrast, in humid climates (Singapore) the consumption was quite low (348 m^3), and quite similar to Carpentras (250 m^3), while the external conditions were more extreme in Singapore. Outdoor air humidity reduced the energy for water evaporation. At the same time, the fan consumption of the system was greater for the climate of Singapore (36 997 kWh) and 20 % more than in Abu Dhabi (30 841 kWh). Therefore, in humid climates, the system consumed little water but a lot of fan energy, while in the subtropical climate the phenomenon was inversed.

The absolute value of performance indicators like α, $SET^*_{dailymax}$, $\Delta SETH/C_{fan}$ and $\Delta SETH/V_w$ are presented on a histogram (Fig. 17).

Fig. 17 shows the absolute values of the performance indicators. We notice that the difference between the exterior conditions of the French (Carpentras and Paris), equatorial (Singapore) and arid subtropical (Abu Dhabi) climates impacts the performance of the system and the interior discomfort of the building. The daily maximum average during occupancy ($SET^*_{dailymax}$) was highest in Abu Dhabi (41.7 °C). Furthermore, the gain in *SETH* per volume of evaporated water was highest for the climate of Singapore at 22.53 °Ch/m^3, which is 54 % more than Abu Dhabi and 49 % more than Carpentras. This shows that in a humid climate, the system reduced indoor discomfort more effectively while consuming the least amount of water. A comparative analysis of the degree-hours gained relative to fan consumption indicated that Carpentras (0.25 °Ch/kWh) and Abu Dhabi (0.24 °Ch/kWh) had more conducive climates than Singapore (0.21 °Ch/kWh). For arid climates, the system helped reduce indoor discomfort with minimal energy consumption by the fan. Finally, we note that for the climate of Singapore alone, the system didn't manage to eliminate the external thermal constraint ($\alpha > 1$).

Finally, we plotted the relative values of these indicators on a radar diagram (Fig. 18). Relative performance maxima (100 %) were specifically set for the $\Delta SETH/C_{fan}$ and $\Delta SETH/V_w$ indicators, given the maximum performance we obtained for these two indicators using simulations in a set of various locations (midterm periods). We therefore obtained the maximum performance for the Buenos Aires site for the indicator $\Delta SETH/V_w = 31.56$ °Ch/m^3, and the maximum performance for the city of Carpentras for $\Delta SETH/C_{fan} = 0.25$ °Ch/kWh.

Fig. 18 shows that the system was more efficient in Paris compared to the other cities studied. The surface of the curve for Paris is slightly larger than that of Carpentras, particularly for the gain in degree hours (T_{op} and *SET**) compared to the reference case. The daily maximum perceived cooling was the best for the climate in Paris (36 %) and the worst in Abu Dhabi (14 %). The trend was a same with the overheating escalation factor: it was the best for the climate in Paris (85 %) but the worst in Singapore (41 %). The extreme climates of Abu Dhabi and Singapore were the least suited to the system studied, particularly because of the high external temperatures all year round. However, we note that for humid climates (Singapore), the gain in discomfort compared to the consumption of evaporated water was the best. For these climates, high water evaporation energy was not necessary to reduce indoor discomfort.

4.3. Climate change

In this part, the impact of climate change on the system operation was studied, and in particular its ability to reduce indoor thermal discomfort. Two different weather files (actual and midterm period)

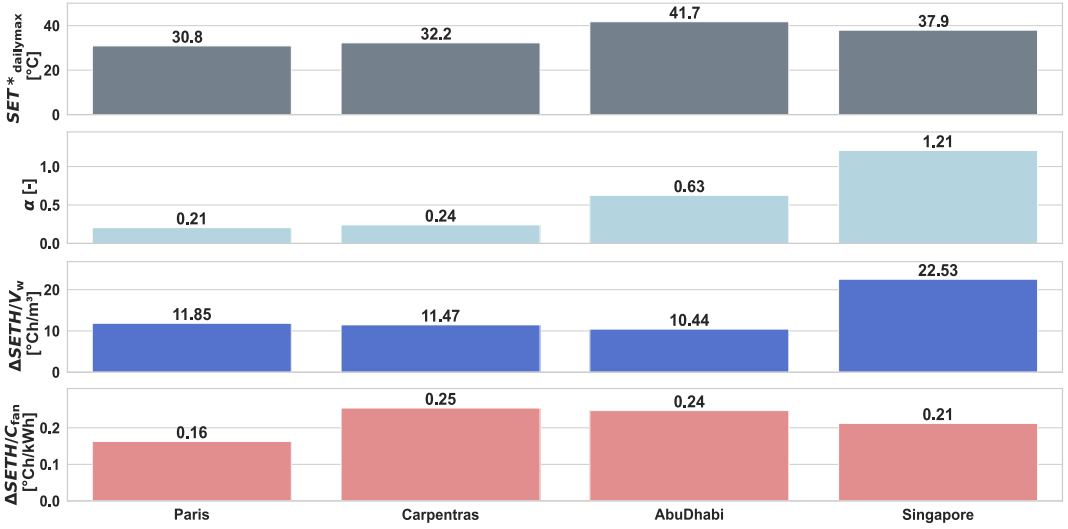

Fig. 17. Quantitative analysis of different indicators (performances).

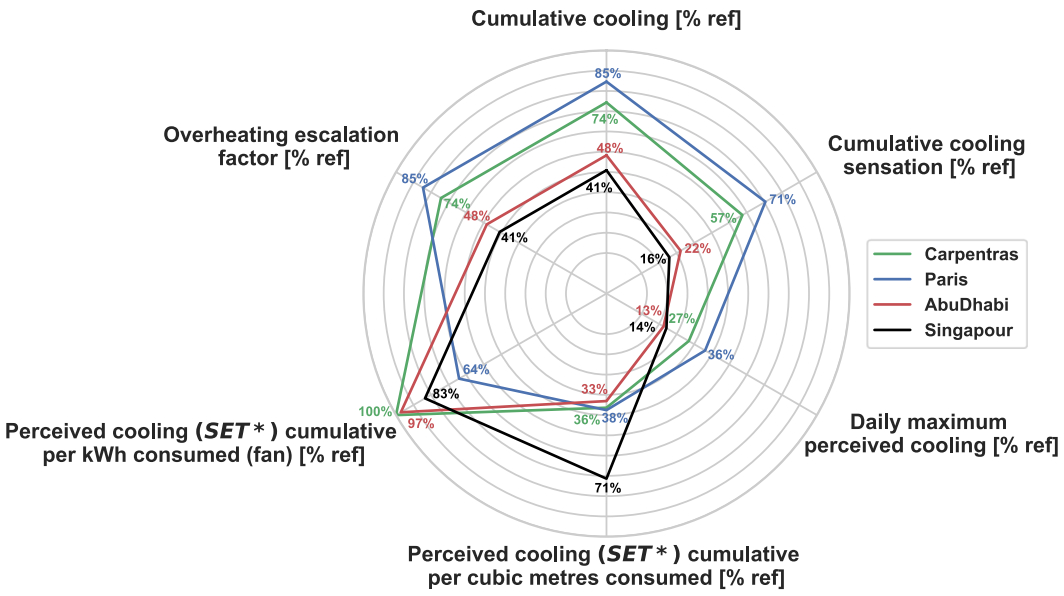

Fig. 18. Radar chart representing system performance for different climates.

were used for Carpentras.

4.3.1. Weather conditions

Outdoor conditions (temperature and relative humidity) were plotted as a heatmap with the days of the year on the x-axis and the hours of the day on the y-axis (Fig. 19).

Fig. 19 illustrates the disparity between historical and projected future meteorological conditions. The analysis indicates an increase in nighttime temperatures in the future weather scenario compared to historical data. While the seasonal trend remains unchanged, characterized by periods of intense heat from late May to early October, the average annual temperature significantly increases in the future scenario, showing an increase of 2 °C. The maximum temperature is 37 °C for the historical period and 41 °C for the future period. At the same time, the average relative humidity over the year decreases by 2 points in the future scenario.

4.3.2. System operation

The operating modes of the system were analyzed for the Carpentras climate under two different weather conditions (historical typical and future typical). The results are presented in the form of various maps, illustrating the system mode operating hours and the percentage fan operation based on days (x-axis) and hours (y-axis).

Fig. 20 shows that free-cooling was most frequently employed during unoccupied periods, while adiabatic cooling took over during occupied periods, especially when free-cooling had not sufficiently cooled the interior of the building. However, the free-cooling occupied periods during the historical period shifted to adiabatic mode for the future period due to the increase in exterior and interior temperature.

It was also observed that for future weather conditions, the use of both modes was more pronounced in terms of both operating hours and fan airflow rates. In the historical weather data, free-cooling (1 282 h) was used more than adiabatic cooling (1 009 h). However, this trend reversed with changing meteorological periods, with 1605 h of adiabatic operation and 1 526 h of free-cooling for future weather conditions. The free-cooling operating time increased by 16 %, while the adiabatic operating time increased significantly by 59 %.

This increase in operating time also led to significant changes in energy consumption, with pump consumption increasing by 60 %, from 40 kWh in the historical period to 64 kWh in the future period. As a result, the total annual energy consumption increased by 51 %, from 6 317 kWh to 9 568 kWh. The increase in the operating time of the adiabatic mode led to an increase in the amount of evaporated water, from 80 m^3 to 181 m^3. Taking into account the drain cycles, the annual water consumption increased by 2.2 times, from 152 m^3 to 345 m^3 per year.

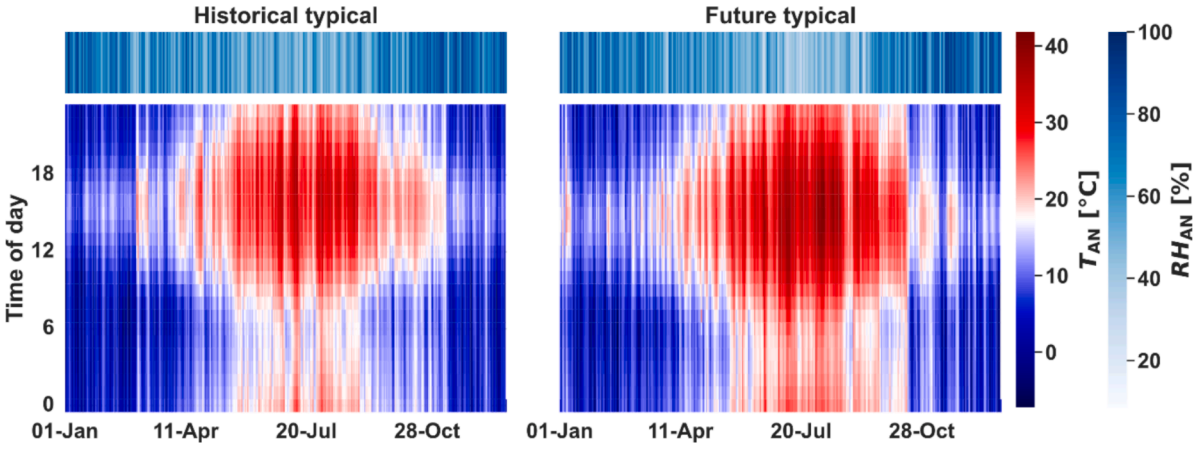

Fig. 19. Outdoor conditions for the city of Carpentras for a typical historical and future weather.

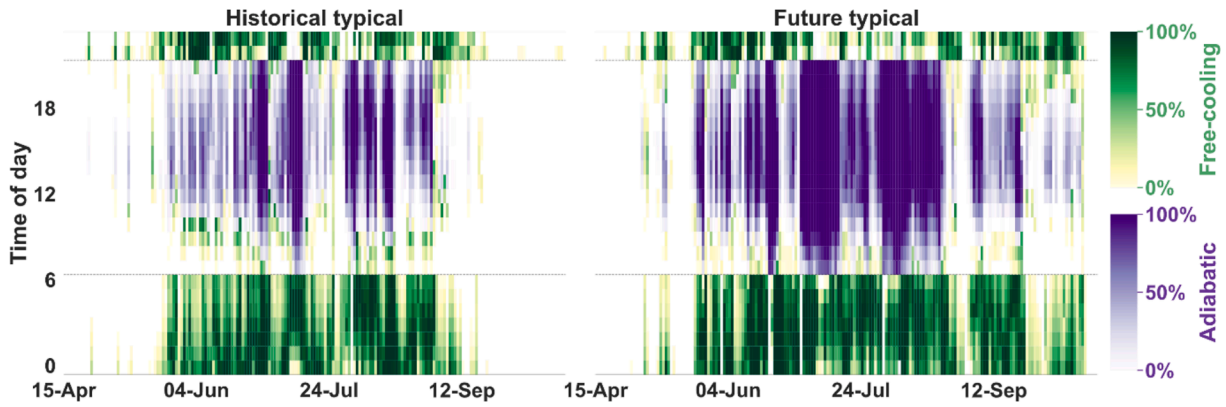

Fig. 20. Analysis of the operation of the two system modes.

4.3.3. Thermal comfort

Fig. 21 presents the *SET** indicator for the climate of Carpentras for historical and future weather scenarios. The results are displayed on various heatmaps representing indoor overheating with a color gradient based on the intensity of this overheating. The days of the year are depicted on the x-axis, and the hours of the day on the y-axis. For each weather period, the upper figure illustrates indoor overheating without the system, while the lower figure represents indoor overheating with the system.

In the absence of the system, we observed a significant increase in the length and intensity of daily overheating periods in future weather forecasts. This trend was particularly evident in the months of July and August. The number of degree hours in the future climate was almost three times that of the historical climate, largely due to external inputs. Furthermore, it's notable that the impact of the system on reducing indoor discomfort decreased when considering future weather forecasts. The observed reduction was 69 % (from 751 °Ch to 234 °Ch) for current weather, compared to 61 % (from 2 344 °Ch to 914 °Ch) for future weather.

We then analyzed the efficiency of the system using comfort and performance indicators. The absolute values of these indicators are shown in Table 7.

We note that the number of degree hours (*DH*) remained very high for the typical future period (5 266°Ch), more than 2.4 times higher than the typical historical period (2 128 °Ch). Consequently, the average daily maximum *SET** for the year was 32.5 °C for the future weather period and 31.4 °C for the historical weather period (+1.1 °C). The gain in degree-hours per kWh consumed by the fan was greater in the future climate, reaching 0.14 °Ch/kWh, an improvement of 0.06 points compared with the historical climate. Similarly, for the reduction in *SETH* in relation to the volume of water evaporated, the system performed better in the future climate, with a gain of 7.7 °Ch/m^3, compared with 6.22 °Ch/m^3 in the historical climate. It can also be seen that the system is well adapted to climate change, particularly by observing the resilience indicator α, which remained low ($\alpha < 1$), despite taking into account a typical future climate scenario.

Table 7
Absolute performance value for two weather periods.

	Historical	Future
DH [°Ch]	246 *(2128)*	1019 *(5266)*
SETH [°Ch]	234 *(751)*	914 *(2344)*
$SET^*_{dailymax}$ [°C]	30.2 *(31.4)*	30.9 *(32.5)*
$\Delta SETH/C_{fan}$ [°Ch/kWh]	0.08	0.14
$\Delta SETH/V_w$ [°Ch/m^3]	6.22	7.7
α [-]	0.078 *(0.679)*	0.132 *(0.685)*

Finally, a comparison of the system performance for two weather periods (typical historical and typical future) was made using a radar graph (Fig. 22). To define the maxima (100 %) of the $\Delta SETH/V_w$ and $\Delta SETH/C_{fan}$ values on this diagram, we took the highest value among all the locations for the historical and future weather periods. In this case, we found values of 35.26 °Ch/m^3 and 0.85 °Ch/kWh, respectively, for the city of Singapore.

Fig. 22 shows that the system was most effective under typical future weather conditions. The relative values obtained show that the difference between the two weather periods was small regarding the reduction in indoor discomfort. The cumulative cooling section shows that the system significantly reduced indoor degree hours (*DH*), with a reduction of 88 % in a historical climate and 81 % in a future climate. The results were slightly worse when the *SET** was considered in the comfort analysis (cumulative cooling sensation), with a difference of 19 points compared with the cumulative cooling for the historical climate (69 %).

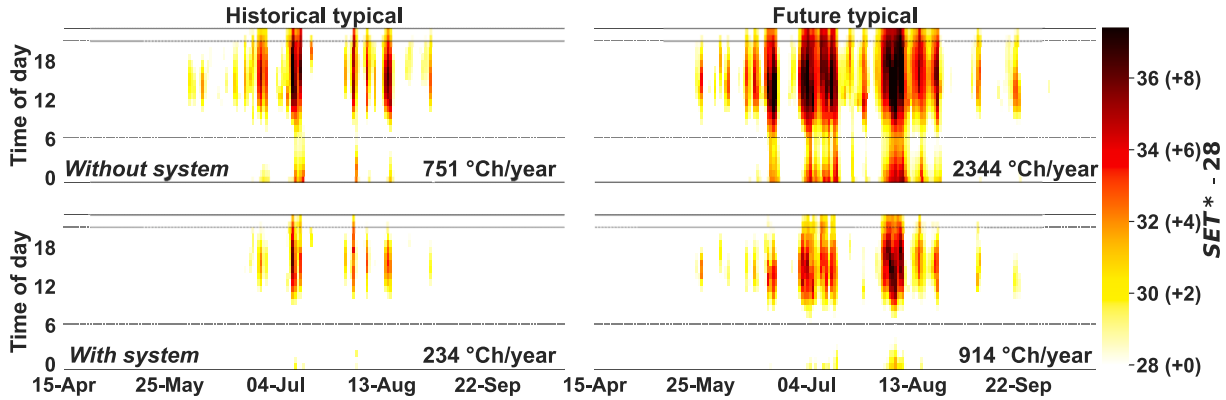

Fig. 21. Internal overheating (SET*−SET*$_{lim}$).

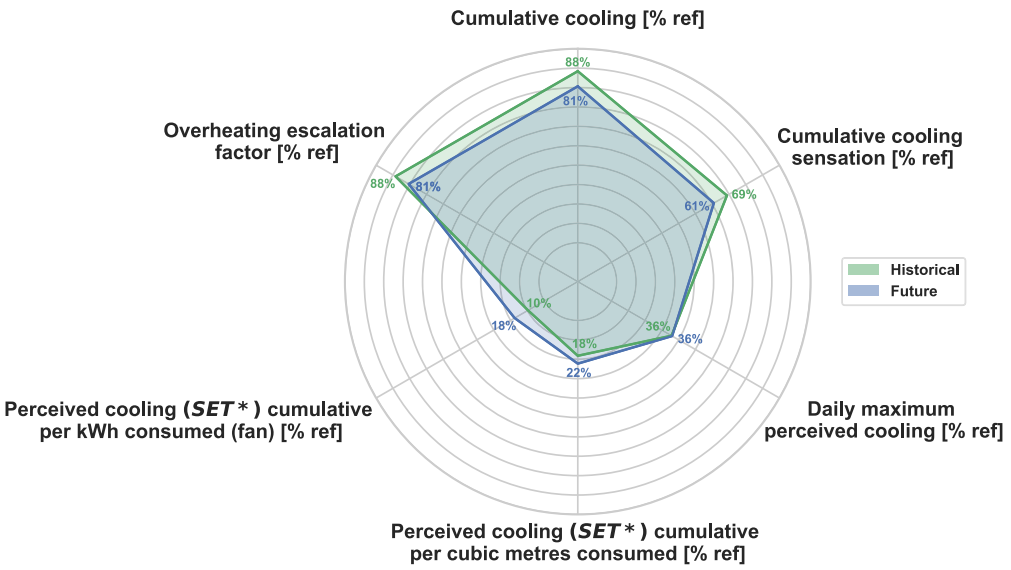

Fig. 22. Radar chart representing system performance for two weather periods.

However, the system still performed well in future weather conditions. By comparing performance indicators, we can see that the system was more efficient in a future climate. The gain in degree-hours per cubic meter of water evaporated ($\Delta SETH/V_w$) was 8 points higher in a future climate than in a historical climate. In a warmer, drier climate, the evaporation phenomenon was amplified, improving the effectiveness of system in reducing indoor discomfort. This trend was also seen when we related this gain in degree hours to the electricity consumption $\Delta SETH/C_{fan}$, the system performing slightly better in a future climate (22 % compared with 18 % in a historical climate). These results indicate that the system performed better in an arid climate and under extreme weather conditions. In addition, the system is expected to be more effective in future years with significantly more challenging external conditions.

5. Conclusions

The objective of this study was to analyze the performance of a direct adiabatic system incorporated into an industrial building under different climates and weather periods using several performance and comfort indicators.

Firstly, the performance of the system was studied for a scorching climate in a French city (Carpentras). The results showed that the system performed better with both modes enabled, significantly reducing internal discomfort (*DH*). The addition of the adiabatic mode made it possible to reduce interior discomfort 3.9 times more (−74 %) compared to the case where free-cooling worked alone (−25 %). These results confirm previous studies on the subject, including those of Chiesa and al. [16], which examined the impact of a direct cooling system on reducing discomfort in a Mediterranean climate, and Guan and al. [45], who explored the cooling potential of a direct system in Australian climates. Taking humidity into account in the analysis of indoor comfort (*SET**) shows that blowing humid air through the system increased indoor humidity and degraded indoor thermo-hydric comfort. The system was more resilient with both modes working.

Subsequently, the impact of the localization on the system was studied. The results show that French climates were the most suitable for this system, particularly for the reduction in discomfort, which was greater (*DH* and *SETH*). The results show that for humid climates (Singapore), the system significantly reduced indoor discomfort by consuming very little water (22.42 °Ch/m^3), unlike arid climates like Abu Dhabi (10.21 °Ch/m^3, −54 %). In arid climates, the system helped reduce indoor discomfort by consuming the least amount of energy for the operation of the fan. For all climates, the building was not resilient when the system was inactive. However, once the system was activated, the building acquired long-term resilience to external thermal constraints, except in the climate of Singapore.

Finally, the results of the impact of climate change on system performance show that the system was more efficient and resilient in future external conditions, particularly on the performance of reducing indoor discomfort in relation to water consumption and fan consumption. The reduction in indoor discomfort (*SETH*) was significant for both weather periods, with a 69 % reduction for the historical period and 61 % for the future period.

To conclude, the system as defined in this study made it possible to significantly reduce the interior discomfort of an industrial building despite the fact that blowing humid air increased the thermal-hydric interior discomfort. The system performed better with both operating modes active. French climates are well suited to the system, particularly the climate of Carpentras. The system was efficient for more extreme climates, particularly in terms of water consumption for humid climates, but the absolute reduction in indoor discomfort was less significant. The system was resilient to predicted climate change, particularly in terms of performance in reducing indoor discomfort in relation to water and fan consumption. Future studies could investigate the performance of the system by modifying the control parameters, especially the setpoint temperature, or by analyzing its efficiency with a different design. In addition, it would be relevant to evaluate the performance of the system in a scenario with a purely indirect adiabatic operation in order to compare its efficiency with that of the current system.

CRediT authorship contribution statement

Antoine Breteau: Writing – review & editing, Writing – original draft, Visualization, Validation, Software, Methodology, Investigation, Formal analysis, Conceptualization. **Emmanuel Bozonnet:** Writing – review & editing, Validation, Supervision, Resources, Project administration, Methodology, Funding acquisition, Formal analysis, Conceptualization. **Patrick Salagnac:** Writing – review & editing, Validation, Supervision, Resources, Project administration, Methodology, Funding acquisition, Formal analysis, Conceptualization. **Jean-Marie Caous:** Supervision, Resources, Project administration, Funding acquisition, Conceptualization.

Declaration of competing interest

The authors declare that they have no known competing financial interests or personal relationships that could have appeared to influence the work reported in this paper.

Acknowledgement

This study was funded by the National Association of Research and Technology (ANRT, France) (Project grant No. 2022/1087).

Appendix

System operation on two representative days, winter and summer, is illustrated in Fig. 24 and Fig. 23 respectively.

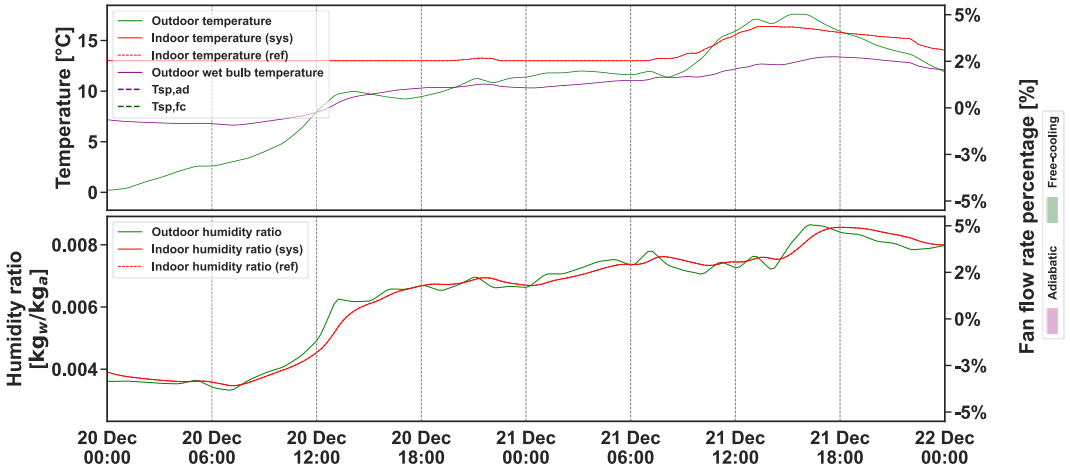

Fig. 23. System operation over 2 consecutive days (winter season).

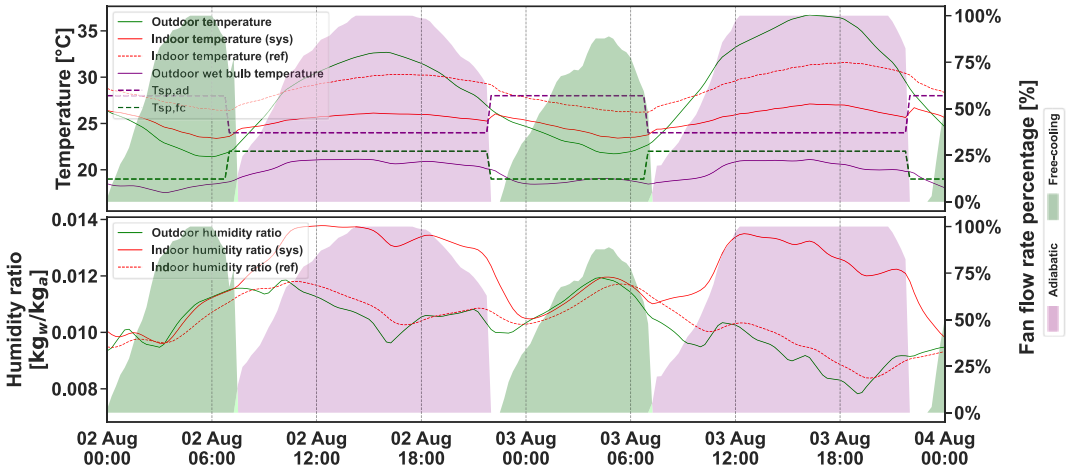

Fig. 24. System operation over 2 consecutive days (summer season).

Data availability

The data that has been used is confidential.

References

[1] WMO confirms that 2023 smashes global temperature record, World Meteorological Organization (2024). https://wmo.int/media/news/wmo-confirms-2023-smashes-global-temperature-record (accessed June 18, 2024).
[2] Global heat pump sales continue double-digit growth – Analysis, IEA (2023). https://www.iea.org/commentaries/global-heat-pump-sales-continue-double-digit-growth (accessed October 15, 2024).
[3] The global cooling pledge: can the world slash cooling emissions by 68% by 2050?, World Economic Forum (2023). https://www.weforum.org/agenda/2023/10/global-cooling-pledge-slash-cooling-emissions-2050/ (accessed October 15, 2024).
[4] C. Zhang, O.B. Kazanci, R. Levinson, P. Heiselberg, B.W. Olesen, G. Chiesa, B. Sodagar, Z. Ai, S. Selkowitz, M. Zinzi, A. Mahdavi, H. Teufl, M. Kolokotroni, A. Salvati, E. Bozonnet, F. Chtioui, P. Salagnac, R. Rahif, S. Attia, V. Lemort, E. Elnagar, H. Breesch, A. Sengupta, L.L. Wang, D. Qi, P. Stern, N. Yoon, D.-I. Bogatu, R.F. Rupp, T. Arghand, S. Javed, J. Akander, A. Hayati, M. Cehlin, S. Sayadi, S. Forghani, H. Zhang, E. Arens, G. Zhang, Resilient cooling strategies – A critical review and qualitative assessment, Energy Build. 251 (2021) 111312, https://doi.org/10.1016/j.enbuild.2021.111312.
[5] B. Ford, N. Patel, P. Zaveri, M. Hewitt, Cooling without air conditioning: the torrent research centre, Ahmedabad, India, Renew. Energy 15 (1998) 177–182, https://doi.org/10.1016/S0960-1481(98)00150-5.
[6] N. Lechner, Heating, Cooling, Lighting: Sustainable Design Methods for Architects, John Wiley & Sons, 2014.
[7] E. Mckenzie, T. Pistochini, F. Loge, M. Modera, An investigation of coupling evaporative cooling and decentralized graywater treatment in the residential sector, Build. Environ. 68 (2013) 215–224, https://doi.org/10.1016/j.buildenv.2013.07.007.

[8] E. Gómez, F.J. Rey-Martínez, A. Tejero-González, The phenomenon of evaporative cooling from a humid surface as an alternative method for air-conditioning, Int. J. Energy Environ. 1 (2010).
[9] J.R. Watt, Evaporative Air Conditioning Handbook, 3rd ed., Fairmont Press, Lilburn, GA, Upper Saddle River, NJ, 1997.
[10] Y.M. Xuan, F. Xiao, X.F. Niu, X. Huang, S.W. Wang, Research and application of evaporative cooling in China: a review (I) – Research, Renew. Sustain. Energy Rev. 16 (2012) 3535–3546, https://doi.org/10.1016/j.rser.2012.01.052.
[11] P. Kowalski, D. Kwiecień, Evaluation of simple evaporative cooling systems in an industrial building in Poland, J. Build. Eng. 32 (2020) 101555, https://doi.org/10.1016/j.jobe.2020.101555.
[12] PROFEEL, Les solutions de rafraichissement adiabatique dans les bâtiments tertiaires en rénovation, Profeel (2021). https://programmeprofeel.fr/ressources/guide-les-solutions-de-rafraichissement-adiabatique-dans-les-batiments-tertiaires-en-renovation/ (accessed June 20, 2023).
[13] A. Sohani, M. Zabihigivi, M.H. Moradi, H. Sayyaadi, H. Hasani Balyani, A comprehensive performance investigation of cellulose evaporative cooling pad systems using predictive approaches, Appl. Therm. Eng. 110 (2017) 1589–1608, https://doi.org/10.1016/j.applthermaleng.2016.08.216.
[14] (PDF) Performance Enhancement by Using Wet Pad in Vapor Compression Cooling System, ResearchGate (2024). https://doi.org/10.5614/j.eng.technol.sci.2019.51.1.4.
[15] E. Hajidavalloo, H. Eghtedari, Performance improvement of air-cooled refrigeration system by using evaporatively cooled air condenser, Int. J. Refrig. 33 (2010) 982–988, https://doi.org/10.1016/j.ijrefrig.2010.02.001.
[16] G. Chiesa, N. Huberman, D. Pearlmutter, M. Grosso, Summer discomfort reduction by direct evaporative cooling in southern mediterranean areas, Energy Procedia 111 (2017) 588–598, https://doi.org/10.1016/j.egypro.2017.03.221.
[17] A. Breteau, P. Salagnac, E. Bozonnet, M. Carage, J.-M. Caous, Evaluation des performances énergétiques d'un système de rafraîchissement adiabatique intégré au sein d'un bâtiment industriel, in: Colloque International Franco-Québécois En Energie Ville et Transition Face Aux Défis Climatiques et Énergétiques, Paris, France, 2022: pp. 164–169. https://hal.archives-ouvertes.fr/hal-03718248 (accessed December 28, 2022).
[18] A. Breteau, P. Salagnac, E. Bozonnet, M. Carage, J.-M. Caous, Comparaison d'indicateurs dans l'analyse du confort intérieur d'un bâtiment industriel équipé d'un système de rafraîchissement adiabatique direct, in: 31ème Congrès Français de La Société Française de Thermique "Thermique et Agroressources", Société Française de Thermique, Reims, France, 2023: p. 127. https://hal.science/hal-04113120 (accessed June 18, 2024).
[19] G.J. Bom, Evaporative Air-conditioning: Applications for Environmentally Friendly Cooling, World Bank Publications, 1999.
[20] I.M. Baca, S.M. Tur, J.N. Gonzalez, C.A. Román, Evaporative cooling efficiency according to climate conditions, Procedia Eng. 21 (2011) 283–290, https://doi.org/10.1016/j.proeng.2011.11.2016.
[21] L. Guan, Implication of global warming on air-conditioned office buildings in Australia, Build. Res. Inf. 37 (2009) 43–54, https://doi.org/10.1080/09613210802611025.
[22] J.R. Camargo, C.D. Ebinuma, J.L. Silveira, Experimental performance of a direct evaporative cooler operating during summer in a Brazilian city, Int. J. Refrig 28 (2005) 1124–1132, https://doi.org/10.1016/j.ijrefrig.2004.12.011.
[23] M.A. Mussa, I.M. Ali Aljubury, W.S. Sarsam, Experimental and analytical study of the energy and exergy performance for different evaporative pads in hot and dry climate, Results Eng. 21 (2024) 101696, https://doi.org/10.1016/j.rineng.2023.101696.
[24] A. Tejero-González, A. Franco-Salas, Optimal operation of evaporative cooling pads: a review, Renew. Sustain. Energy Rev. 151 (2021) 111632, https://doi.org/10.1016/j.rser.2021.111632.
[25] I. Kovačević, M. Sourbron, The numerical model for direct evaporative cooler, Appl. Therm. Eng. 113 (2017) 8–19, https://doi.org/10.1016/j.applthermaleng.2016.11.025.
[26] A. De Angelis, M. Medici, O. Saro, G. Lorenzini, Evaluation of evaporative cooling systems in industrial buildings, Int. J. Heat Technol. 33 (2015) 1–10, https://doi.org/10.18280/ijht.330301.
[27] NF EN 12831-1, Afnor EDITIONS (n.d.). https://www.boutique.afnor.org/fr-fr/norme/nf-en-128311/performance-energetique-des-batiments-methode-de-calcul-de-la-charge-thermi/fa184817/79485 (accessed April 20, 2023).
[28] Chapitre II : Aération, assainissement (Articles R4222-1 à R4222-26) - Légifrance, (n.d.). https://www.legifrance.gouv.fr/codes/section_lc/LEGITEXT000006072050/LEGISCTA000018488858/ (accessed September 27, 2023).
[29] E.H. Mathews, M. Kleingeld, L.J. Grobler, Integrated simulation of buildings and evaporative cooling systems, Build. Environ. 29 (1994) 197–206, https://doi.org/10.1016/0360-1323(94)90070-1.
[30] S.V. Mehere, K.P. Mudafale, D.S.V. Prayagi, Review of Direct Evaporative Cooling System With Its Applications, 2 (2014) 5.
[31] C. Zhang, O.B. Kazanci, S. Attia, R. Levinson, S.H. Lee, P. Holzer, R. Rahif, A. Salvati, A. Machard, M. Pourabdollahtootkaboni, A. Gaur, B. Olesen, P. Heiselberg, IEA EBC Annex 80 - Dynamic simulation guideline for the performance testing of resilient cooling strategies: Version 2, Department of the Built Environment, Aalborg University, Aalborg, 2023.
[32] A. Machard, C. Inard, J.-M. Alessandrini, C. Pelé, J. Ribéron, A methodology for assembling future weather files including heatwaves for building thermal simulations from the European coordinated regional downscaling experiment (EURO-CORDEX) climate data, Energies 13 (2020) 3424, https://doi.org/10.3390/en13133424.
[33] P. Holzer, IEA EBC Annex 80 - Resilient Cooling, (n.d.). https://annex80.iea-ebc.org/.
[34] T. Kusuda, P.R. Achenbach, Earth temperature and thermal diffusivity at selected stations in the United States, in: 0 ed., National Bureau of Standards, Gaithersburg, MD, 1965: p. NBS report; 8972. https://doi.org/10.6028/NBS.RPT.8972.
[35] E. ISO, 10211: 2017 Thermal bridges in building construction—Heat flows and surface temperatures—Detailed calculations, 2017.
[36] ASHRAE, ANSI/ASHRAE Standard 55-2013, (2013).
[37] D. Enescu, A review of thermal comfort models and indicators for indoor environments, Renew. Sustain. Energy Rev. 79 (2017) 1353–1379, https://doi.org/10.1016/j.rser.2017.05.175.
[38] C.E.A. Winslow, L.P. Herrington, A.P. Gagge, The relative influence of radiation and convection upon the temperature regulation of the clothed body, Am. J. Physiol.-Legacy Content 124 (1938) 51–61, https://doi.org/10.1152/ajplegacy.1938.124.1.51.
[39] R.J. de Dear, A global database of thermal comfort field experiments, (1998). https://www.osti.gov/biblio/649444 (accessed November 18, 2022).
[40] A. Gagge, A. Fobelets, L. Berglund, A standard predictive index of human response to the thermal environment, ASHRAE Trans. 92 (1986) 709–731.
[41] S. Zare, N. Hasheminejad, H.E. Shirvan, R. Hemmatjo, K. Sarebanzadeh, S. Ahmadi, Comparing universal thermal climate index (UTCI) with selected thermal indices/environmental parameters during 12 months of the year, Weather Clim. Extremes 19 (2018) 49–57, https://doi.org/10.1016/j.wace.2018.01.004.
[42] S. Attia, R. Rahif, V. Corrado, R. Levinson, A. Laouadi, L. Wang, B. Sodagar, A. Machard, R. Gupta, B. Olesen, M. Zinzi, P. Heiselberg, M. Hamdy, Framework to evaluate the resilience of different cooling technologies, 2021. https://doi.org/10.13140/RG.2.2.33998.59208.
[43] M. Hamdy, S. Carlucci, P.-J. Hoes, J.L.M. Hensen, The impact of climate change on the overheating risk in dwellings—A Dutch case study, Build. Environ. 122 (2017) 307–323, https://doi.org/10.1016/j.buildenv.2017.06.031.
[44] S. Flores-Larsen, C. Filippín, F. Bre, New metrics for thermal resilience of passive buildings during heat events, Build. Environ. 230 (2023) 109990, https://doi.org/10.1016/j.buildenv.2023.109990.
[45] L. Guan, M. Bennett, J. Bell, Evaluating the potential use of direct evaporative cooling in Australia, Energy Build. 108 (2015) 185–194, https://doi.org/10.1016/j.enbuild.2015.09.020.